RADIO SCIENCE, VOL. 38, NO. 4, 8060, doi:10.1029/2002RS002637, 2003

Issues concerning the sea emissivity modeling at L band for retrieving surface salinity

Emmanuel P. Dinnat and Jacqueline Boutin

Laboratoire d'Océanographie Dynamique et de Climatologie, Paris, France

Gérard Caudal

Centre d'étude des Environnements Terrestres et Planétaires, Vélizy, France

Jacqueline Etcheto

Laboratoire d'Océanographie Dynamique et de Climatologie, Paris, France

Received 5 March 2002; revised 11 June 2002; accepted 20 August 2002; published 27 May 2003.

[1] In order to prepare the sea surface salinity (SSS) retrieval in the frame of the Soil Moisture and Ocean Salinity (SMOS) mission we conduct sensitivity studies to quantify uncertainties on simulated brightness temperatures (T_b) related to uncertainties on sea surface and scattering modeling. Using a two-scale sea surface emissivity model to simulate T_b at L band (1.4 GHz), we explore the influence on estimated SSS of the parameterization of the seawater permittivity, of the sea wave spectrum, of the choice of the two-scale cutoff wavelength, and of adding swell to the wind sea. Differences between T_b estimated with various existing permittivity models are up to 1.5 K. Therefore a better knowledge of the seawater permittivity at L band is required. The influence of wind speed on T_b simulated with various parameterizations of the sea wave spectrum differs by up to a factor of two; for a wind speed of 7 m s^{-1} the differences on estimated SSS is several psu depending on the sea wave spectral model taken, so that sea spectrum is a major source of uncertainty in models. We find no noticeable effect on simulated T_b when changing the two-scale cutoff wavelength and when adding swell to the wind sea for low to moderate incidence angles. The dependence of the wind-induced T_b on SST and SSS being weak, we assess the error in SSS estimated assuming that the wind speed influence is independent of SST and SSS. We find errors on estimated SSS up to 0.5 psu for 20°C variation in SST. Therefore this assumption would induce regional biases when applied to global measurements. *INDEX TERMS:* 4275 Oceanography: General: Remote sensing and electromagnetic processes (0689); 4271 Oceanography: General: Physical and chemical properties of seawater; 0659 Electromagnetics: Random media and rough surfaces; *KEYWORDS:* microwave, radiometry, remote sensing, salinity, roughness

Citation: Dinnat, E. P., J. Boutin, G. Caudal, and J. Etcheto, Issues concerning the sea emissivity modeling at L band for retrieving surface salinity, *Radio Sci.*, *38*(4), 8060, doi:10.1029/2002RS002637, 2003.

1. Introduction

[2] Ocean salinity is a key parameter of the oceanic circulation, which plays an important role in the climate system. Together with temperature, salinity determines the density of water masses which drives the thermohaline circulation. Sea Surface Salinity (SSS) is also a tracer of the water cycle, as it is affected by precipitation and evaporation. However, until now there is a lack of measurements of SSS over large areas of the global ocean and a lack of long-term SSS monitoring. The Soil Moisture and Ocean Salinity (SMOS) mission is the first attempt to globally monitor SSS by satellite [*Kerr et al.*, 1998]. The SMOS instrument will perform multiangular and multipolarization L band (1.4 GHz) brightness temperature (T_b) measurements by means of a 2D synthetic aperture antenna. With decreasing frequency,

0048-6604/03/2002RS002637$11.00

the sensitivity of T_b to SSS increases and the spatial resolution decreases; L band is a trade-off between both the accuracy and resolution constraints. The threshold accuracy in SSS required for oceanic studies, as recommended by the Global Ocean Data Assimilation Experiment (GODAE) group, is 1 practical salinity unit (psu) on salinity integrated over a 200 $\times$ 200 km pixel and over 10 days, the optimized accuracy being 0.1 psu.

[3] In order to invert satellite-based measurements, empirical models are usually developed to relate satellite-based data to geophysical parameters. However in the present case, the lack of both SSS data and L band radiometric measurements over large regions of the global ocean prevents from proceeding in that way. SSS measurements are sampled along commercial ship tracks or during time- and space-limited oceanographic campaigns, resulting in a relatively poor spatial and temporal sampling of global ocean SSS. Radiometry at L band was until now mostly used in radio astronomy and not in remote sensing of the oceans, because of the difficulty to achieve an acceptable spatial resolution for oceanic studies, resulting in a relatively poor knowledge of the open sea emissivity at low frequency. SMOS will be the first satellite-borne L band radiometer, providing the first L band emissivity measurements at global scale.

[4] Studies are underway to optimize the SMOS antenna design and the measurements strategy in order to minimize the error on the retrieved SSS [e.g., *Waldteufel et al.*, 2003; *Waldteufel and Caudal*, 2002; *Johannessen et al.*, 2002]. These studies necessitate a model to simulate the sensitivity of T_b to geophysical parameters such as SSS, sea surface temperature (SST) and wind velocity ($\vec{U}$). Some empirical emissivity models have been developed to relate emissivity measurements to geophysical parameters, mostly at high frequencies where numerous satellite data are available. At L band, *Sasaki et al.* [1987] derived the wind influence on emissivity by combining L band observations made over a canal [*Swift*, 1974], the Bering Sea [*Webster and Wilheit*, 1976] and from the Argus Island Tower [*Hollinger*, 1971]. However, in the open sea, the sea state is likely to be different so it is uncertain that such measurements can lead to an empirical law applicable to the global ocean. In this context, recent campaigns of L band radiometric measurements were conducted on behalf of ESA to refine sea surface emissivity models (WISE 2000, WISE 2001, EuroSTARRS), especially concerning the wind effect on T_b which is uncertain at low frequency. Recently, *Yueh et al.* [2001] showed that an empirical correction of the wind influence on T_b is possible using normalized radar cross section (σ_0) measurements. However SMOS will provide only passive measurements, and it will be much easier to co-locate them with wind speeds derived for instance from meteorological-models than with active measurements. Therefore, although this approach appears promising, it is not discussed in the present paper; we focus on theoretical modeling of the sea emissivity which offers the opportunity to understand the relative influence of the various parameters in the emissivity process. Of course, it does not rule out the need of calibration/validation studies to derive semi-empirical models for operational applications. A general discussion about error sources when estimating SSS from radiometric measurements at L band has been given by *Yueh et al.* [2001], who assessed the influence on T_b of the atmosphere, the clouds, the ionosphere and the solar system/galactic radiations.

[5] Theoretical models were developed and validated at high frequencies (e.g., 19 GHz and 37 GHz) where they are used to retrieve wind speed or atmospheric parameters for example, and where there is almost no influence of SSS on T_b. Theoretical modeling necessitates a description of the seawater permittivity, of the sea waves and of the scattering processes induced by a rough surface (here the wind-roughened sea surface). We test various parameterizations in an emissivity model in order to evaluate discrepancies in simulated T_b and assess whether the resulting SSS discrepancies are acceptable for oceanic studies. We pay a particular attention to discrepancies at incidence angles smaller than 40°, because they represent most of the SMOS incidence angles (i.e., 80% of them). Figure 1 reports incidence angles statistics for the pixels in the SMOS field of view.

[6] Various electromagnetic models exist to simulate emissivity from sea surface. We use a two-scale model because of its relative efficiency to simulate the wind influence at small incidence angles in the microwave domain with respect to a geometrical optics model and because of its low computation time with respect to a rigorous solution of the Maxwell equations [*Dinnat et al.*, 2002]. At given polarization and incidence angle (θ), we expand T_b in two terms: $T_{b\,flat}$, for a flat surface which does depend neither on wind speed (U) nor wind direction (ϕ) and $T_{b\,wind}$, which is a correction term to $T_{b\,flat}$ due to surface roughness induced by the wind:

$$T_b = T_{b\,flat}(\epsilon(SST, SSS)) + T_{b\,wind}(\epsilon(SST, SSS), U, \phi) \quad (1)$$

where ϵ is the seawater permittivity.

[7] $T_{b\,flat}$ is a function of ϵ, which depends on SSS and SST. In section 2, we evaluate the discrepancies between $T_{b\,flat}$ simulated with various ϵ models, and the differences in SSS estimated with various ϵ models. We discuss to what extent it is possible to reduce the SSS uncertainty by calibrating the T_b measured by the radiometer.

[8] The computation of $T_{b\,wind}$ is derived from the two-scale electromagnetic model of *Yueh* [1997]; small sea

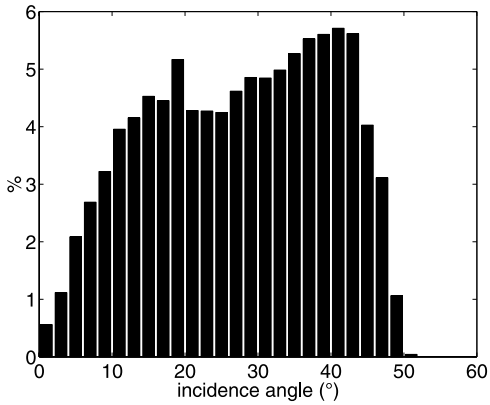

Figure 1. Distribution of the incidence angles for the pixels in the SMOS field of view.

waves (which induce Bragg scattering) are superimposed on large sea waves (which reflect electromagnetic waves as infinite planes). Results of this model agree with measurements performed at S- and L band by *Hollinger* [1971], *Blume et al.* [1977] and *Wilson et al.* [2001] that showed that wind induces noticeable increase in T_b at low frequencies (a few tenths of a Kelvin per m s^{-1}). A precise parameterization of the wind influence is crucial for SSS retrieval. In section 3 we study the uncertainties on simulated $T_{b\ wind}$ due to uncertainties on sea state parameterization and on emissivity modeling.

2. Simulations of Brightness Temperature for a Flat Sea Surface

[9] The brightness temperature of the sea surface is related to the complex relative permittivity of seawater ϵ that depends on SSS, SST and frequency. Therefore, to estimate SSS from radiometric measurements at L band one needs a model that relates ϵ to SSS and SST and which is valid at 1.4 GHz. Existing ϵ models rely on a semi-empirical approach and have been developed since the 70's. In these models, the dependence of the permittivity on the frequency follows the theoretical *Debye* [1929] equation in which parameters dependent on salinity and temperature are empirically fitted to permittivity measurements.

[10] There are few measurements of the permittivity of natural seawater, especially at low frequency such as 1.4 GHz. *Klein and Swift* [1977] (hereinafter referred to as KS) based their model on data acquired at 1.43 GHz [*Ho et al.*, 1974] and 2.653 GHz [*Ho and Hall*, 1973]. *Stogryn et al.* [1995] (hereinafter referred to as S95) used data between 7 and 14 GHz. *Ellison et al.* [1996] (hereinafter referred to as EL) used data between 3 and 20 GHz and at spot frequencies (23.8, 36.5, and 89 GHz). Finally, *Stogryn* [1997] (hereinafter referred to as S97) used data from *Stogryn et al.* [1995] and *Ellison et al.* [1996]. Models based on NaCl solutions [e.g., *Stogryn*, 1971] are ignored here because the permittivity of NaCl differs noticeably from the one of seawater [*Ellison et al.*, 1996].

[11] There is no convincing evidence that one model should be better at L band than the others. KS model is the only model including measurements at 1.4 GHz, but the authors found that these measurements suffer from a bias so that the claimed accuracies of 0.2% and 0.4% on real and imaginary part of ϵ respectively [*Ho et al.*, 1974] are optimistic. Moreover NaCl samples together with seawater samples were used and few measurements of seawater were performed at salinities encountered in open ocean (most of the measurements were performed in the range 4–30 psu). EL, S95 and S97 models are based on recent ϵ measurements made at frequencies higher than 1.4 GHz. Although the Debye equation provides approximations close to experimental data at low microwave frequencies, the accuracy of these ϵ models at L band is likely to be less than claimed for higher frequencies. Discrepancies between ϵ estimated at 1.4 GHz with these various models are always less than 3% concerning the real part and less than 5% concerning the imaginary part, the largest discrepancies being between EL and KS models (Figure 2). In this section we determine discrepancies in T_b induced by discrepancies in ϵ, focusing exclusively on the L band. The issue is whether these discrepancies are small enough to meet the GODAE requirements and whether these discrepancies can be resolved or at least reduced by T_b calibration/validation of the radiometer.

[12] Assuming thermodynamic equilibrium, $T_{b\ flat}$ is related to the Fresnel reflection coefficient (R) by

$$T_{b\ flat} = \mathrm{SST}(1 - \mathrm{R}(\epsilon, \theta)) \qquad (2)$$

[13] *Dinnat et al.* [2002] showed that there are noticeable discrepancies on $T_{b\ flat}$ when computed either with EL model or with KS model at nadir. Here, we estimate $T_{b\ flat}$ at incidence angles ranging from nadir to 60° using the KS, El, S95 and S97 models, for SST and SSS ranges encountered in the open ocean. According to the Levitus Climatology [*Boyer et al.*, 1998a, 1998b, 1998c; *Antonov et al.*, 1998a, 1998b, 1998c], the mean SSS and SST over the global ocean are 34.8 psu and 18.4°C respectively. The SSS varies from 31 to 38 psu and the SST from −1.8 to 31°C. It must be noted that cold waters (SST less than 10°C) have SSS limited to 35.5 psu: consequently we will not consider large salinity for cold waters.

[14] Over the considered SSS and SST ranges, S97 model differs from S95 by always less than 0.15 K, the discrepancy at the mean oceanic SSS and SST being less

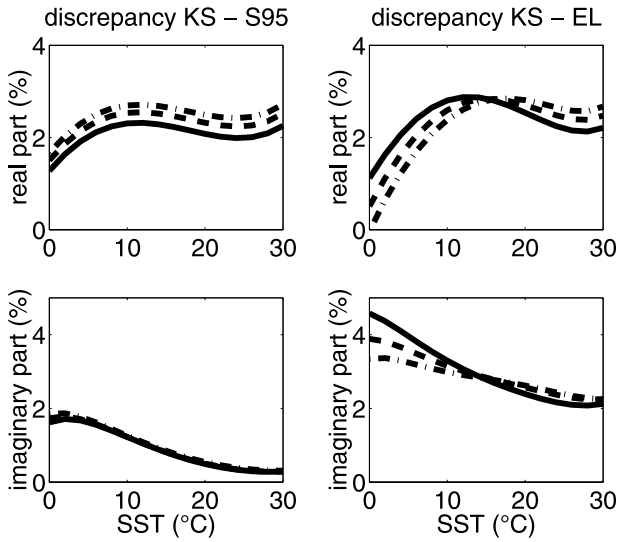

Figure 2. Discrepancies at 1.4 GHz between seawater permittivity estimated with (left) KS-S95 models and (right) KS-EL models (see text for abbreviations) versus sea surface temperature. Sea surface salinity is 31 psu (solid line), 34.8 psu (dashed line) and 38 psu (dashed-dotted line).

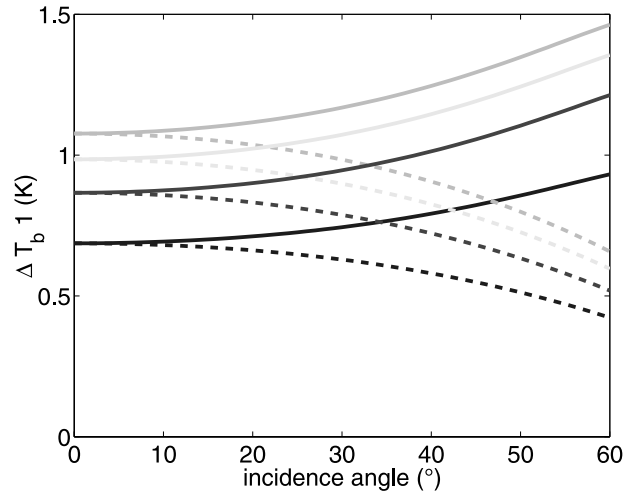

Figure 3. Differences of $T_{b\ flat}$ estimated with EL and KS models (EL-KS) versus the incidence angle, in vertical polarization (solid line) and horizontal polarization (dashed line). Sea surface temperature is 0°C (dark blue), 10°C (light blue), 20°C (yellow) and 30°C (red). See color version of this figure at back of this issue.

than 0.02 K. Therefore S97 and S95 will be considered similar in the following.

[15] Differences between $T_{b\ flat}$ estimated with EL and KS models (ΔT_b1) are reported versus the incidence angle in Figure 3, for the mean oceanic SSS (34.8 psu) and for SST = 0°C (dark blue), 10°C (light blue), 20°C (yellow), and 30°C (red). Likewise, differences between S95 and KS models (ΔT_b2) are reported on Figure 4. The results at other SSS (not shown) are very similar, SSS influence on ΔT_b1 and ΔT_b2 being negligible. Indeed, ΔT_b2 varies by less than 0.1 K (at any SST or incidence angle) over the considered SSS range (not shown). ΔT_b1 variation is also less than 0.1 K for SST warmer than 12°C, and less than 0.25 K (for SSS varying from 31 to 35 psu) for cold water. This small sensitivity of T_b differences to SSS means that the influence of SSS on $T_{b\ flat}$ is in close agreement in the various models, especially between S95 and KS models. Therefore the uncertainty on ϵ parameterization is mainly influenced by SST.

[16] KS model gives always the lowest estimations of $T_{b\ flat}$ (ΔT_b1 and ΔT_b2 are always positive). EL model induces always the largest $T_{b\ flat}$, so that S95 model is always between both the other models. In other words, ΔT_b1 is always larger than ΔT_b2 so it is representative of the maximum uncertainty between various parameterizations. Recent L band campaigns were interpreted using either KS model [e.g., *Le Vine et al.*, 1998; *Miller et al.*, 1998; *Wilson et al.*, 2001] or EL model [e.g., *Yueh et al.*, 2001]. We study the differences between SSS estimated with KS and EL models.

[17] The sensitivity of SSS to $T_{b\ flat}$ ($\partial SSS/\partial T_{b\ flat}$) at nadir ranges from −1.5 psu/K (at SST = 30°C) to −4.5

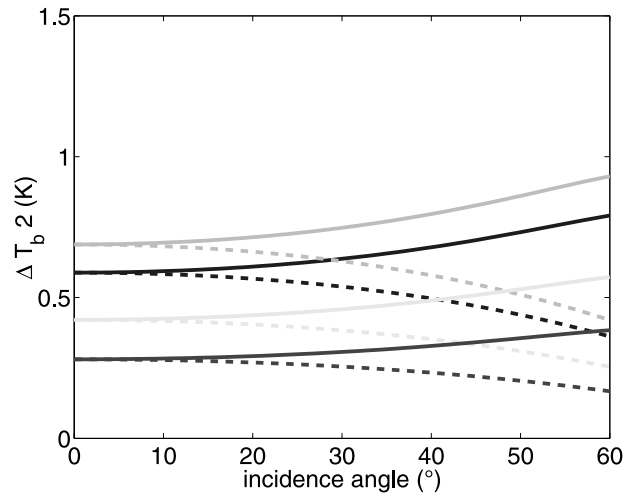

Figure 4. Differences of $T_{b\ flat}$ estimated with S95 and KS models (S95-KS) versus the incidence angle, in vertical polarization (solid line) and horizontal polarization (dashed line). Sea surface temperature is 0°C (dark blue), 10°C (light blue), 20°C (yellow), and 30°C (red). See color version of this figure at back of this issue.

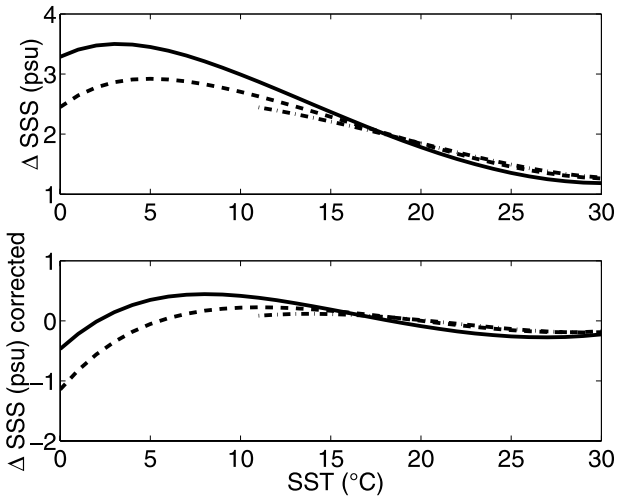

Figure 5. Δ*SSS*, uncertainty on SSS due to uncertainties on parameterization of seawater permittivity, versus SST and for various salinities: 31 (solid line), 34.8 (dashed line), and 38 psu (dashed-dotted line). Incidence angle is 0°. Results for large SSS/cold SST are not reported since these conditions are not realistic in the open ocean. Calibration/validation in T_b is not included (top) or included (bottom).

psu/K (at SST = 0°C) and from −1 to −3.2 psu/K at 60° incidence angle. It is weakly dependent on SSS and on the permittivity model (as seen previously, the influence of SSS on $T_{b\,flat}$ is almost the same whatever model we use). In order to assess the uncertainty in SSS, we compute the differences between SSS estimated from a T_b database with either KS or EL model (ΔSSS). The $T_{b\,flat}$ database is built using KS model (same SSS and SST ranges as previously).

[18] ΔSSS at nadir is reported versus SST for various SSS derived from KS model (Figure 5, top). Differences between SSS estimated with various permittivity models are independent of incidence angle (not shown). They range from 1.2 psu in warm waters (30°C) to 3.3 psu in cold and less salted waters (31 psu, 5°C). They vary almost linearly with SSS in cold waters and are almost independent of SSS for SST warmer than 15°C. In spite of relatively small discrepancy in T_b for cold waters, ΔSSS is large for SST less than 10°C because of the large $\partial SSS/\partial T_{b\,flat}$. $\Delta T_b 1$ is almost constant over a large range of SST and SSS and it could be partially considered as a bias. We study to what extent ΔSSS could be reduced by removing a constant bias on $T_{b\,flat}$, assuming that such a bias could be determined from cal/val measurements. Hence we compute ΔSSS after correcting the $T_{b\,flat}$ in database by the assumed bias; the bias is derived from $\Delta T_b 1$ at SST = 20°C and SSS = 35 psu. The SSS uncertainty strongly decreases and ranges from −1 psu (at 0°C) to 0.4 psu (at 7°C), but is still larger than the required accuracy (Figure 5, bottom). We tested the effect of correcting a bias derived from $\Delta T_b 1$ at various SST. The resulting ΔSSS is always small around the chosen SST but is still of the order of 1 psu for other SST. We concluded that an empirical correction of T_b by calibration/validation independent of SST is not sufficient to correct for the permittivity model uncertainty. Yet the situation could be improved by regional cal/val operations, at least for SST above 5°C.

[19] The accuracy required on permittivity to achieve a 0.1 K accuracy in T_b is of the order of 0.3% [*Dinnat et al.*, 2002]. T_b measurements could provide an empirical validation of the permittivity models at L band, especially concerning the sensitivity to SST. However, the T_b accuracy required is stringent because of the large sensitivity of estimated SSS to T_b (for cold waters, an accuracy better than 0.1 K is required).

3. Simulations of Wind Effect on T_b With a Two-Scale Model

3.1. Model Description

[20] We simulate the wind effect on sea brightness temperature using the two-scale model described by *Yueh* [1997]. In two-scale models, a cutoff wavelength (λ_d) parts the large from the small-scale waves. Large-scale waves are defined as the waves whose horizontal extent greatly exceeds the wavelength of the radiometer (λ_0); therefore these waves can be considered as facets of infinite extent and their emissivity can be computed using geometric optics (GO). These facets are perturbed by small-scale waves, whose height standard deviation is less than λ_0. Therefore the emissivity is corrected for this roughness effect using a second-order small perturbation method (SPM). Various models have been proposed to describe the sea wave spectrum; most of them have been extensively validated by means of microwave measurements in the centimetric wavelength domain but their validity in the L band range remains uncertain. In a standard configuration, we use the *Durden and Vesecky* [1985] spectrum multiplied by a factor of two (referred as DV2 in the following), because this adjustment makes the model in closer agreement with high frequency measurements [*Yueh*, 1997]. In section 3.4, we assess the influence of the discrepancies in various spectra on wind-induced T_b. For this purpose, we use the sea wave spectra from *Durden and Vesecky* [1985] (hereinafter referred to as DxxxxV) and *Elfouhaily et al.* [1997] (hereinafter referred to as Elfo). The omnidirectional component of these spectra is reported in Figure 6, together with the cutoff wavelength at L band taken as λ_d = 80 cm.

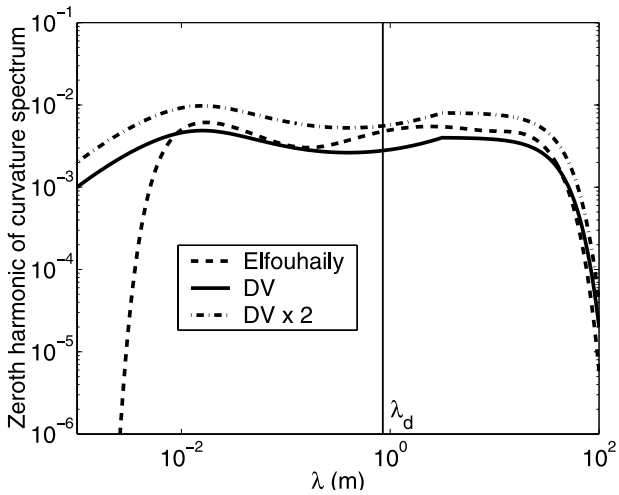

Figure 6. Various omnidirectional curvature spectra (see text). λ_d is the cutoff wavelength.

[21] The upwind-downwind asymmetry in T_b is driven by the hydrodynamic modulation (i.e., there is more roughness on the upwind side). Below $\theta = 30°$, this asymmetry is in close agreement between the simulations with the three spectra, differing by less than 0.1 K.

[22] The upwind-crosswind asymmetry in T_b is driven by the second harmonic of the sea wave spectrum (dependent on the spreading function). The second harmonic of the DV spectrum decreases (with increasing wavelength) from centimetric wavelengths (not shown), whereas the second harmonic of the Elfo spectrum (not shown) decreases for wavelengths much larger than 21 cm (i.e., the wavelength corresponding to 1.4 GHz) because of a long-wavelength peak. Consequently, at 1.4 GHz, the upwind-crosswind asymmetry is much larger with the Elfo spectrum than with DV and DV2 spectra [*Boutin et al.*, 2002], contrary to what occurs at higher frequencies (19 GHz and 37 GHz) [*Zhang and Johnson*, 2001]. At nadir and for a wind speed of 10 m s^{-1}, the upwind-crosswind asymmetry in T_b is less than 0.15 K (peak to peak) with DV and DV2 spectra, whereas it is 0.6 K (peak to peak) with Elfo spectrum. These azimuthal variations being relatively small, they will be ignored in the following studies, where only azimuthally averaged quantities will be considered. Also, as the foam parameterization at L band is very uncertain, foam will not be included in our simulations.

3.2. Decoupling SST and SSS Effect From Wind Effect

[23] Because of the complexity of electromagnetic models used to compute the emissivity of a rough surface, it would be tempting to consider the effect of surface roughness as a perturbation term independent of SSS and SST, to be determined only once for given wind conditions and given incidence angle. In that case the quantity $T_{b\ wind}$ of equation 1 would not depend on ϵ. Some of the empirical models of wind-induced T_b [e.g., *Sasaki et al.*, 1987] make this approximation. We study the influence of SSS and SST on $T_{b\ wind}$ in order to evaluate to what extent it can be neglected when dealing with regional measurements usually taken over a limited range of SSS and SST variations, and when retrieving SSS from satellite measurements at global scale. We assume that $T_{b\ wind}$ is only a function of U and ϕ so that equation 1 of the standard model rewrites for the decoupled model:

$$T_b = T_{b\,flat}(\epsilon(SST, SSS)) + T^*_{b\,wind}(U, \phi) \qquad (3)$$

[24] $T^*_{b\ wind}$ is computed at SST* = 20°C and SSS* = 35 psu.

[25] $T_{b\ wind}$ is weakly sensitive to SSS and SST; for U = 10 m s^{-1} it differs from $T^*_{b\ wind}$ by less than 0.25 K whatever SST and SSS are. However, because of the stringent accuracy required on SSS and of the large sensitivity $\partial SSS/\partial T_b$ for cold waters, these differences may induce noticeable differences in estimated SSS. In order to evaluate the error on the retrieved SSS resulting from assuming $T_{b\ wind}$ independent of SSS and SST, we estimate SSS from T_b (assuming that SST and T_b are perfectly known) using either the decoupled model or the standard model. Differences between estimated SSS with one or the other model (ΔSSS) are reported at nadir for a wind speed of 10 m s^{-1} in Figure 7. The influence of SSS is less than ±0.035 psu while the one of SST is much larger. For waters above 10°C, the SSS error is ±0.1 psu and varies slowly with SST. It amounts to 0.4 psu at 0°C where it is maximum because of the choice of SST* (15°C) and because of the stronger sensitivity of SSS to T_b in cold waters. We computed $T^*_{b\ wind}$ at other SST*. The SSS error (not shown) was always small around SST* but remained several tenths of a psu when the difference SST - SST* was large. The SSS errors computed at other incidence angles are very similar.

[26] When dealing with global ocean measurements, considering that the wind effect is independent of SST would introduce regional biases of several tenths of a psu. Moreover, this bias is not very variable with incidence angle and polarization so that it could not be corrected by a multiangular inversion as proposed for SMOS. However, in the frame of a regional study with limited variations of SST (especially for SST warmer than 10°C), such as the WISE campaign, a $T_{b\ wind}$ constant with SST and SSS could be assumed with

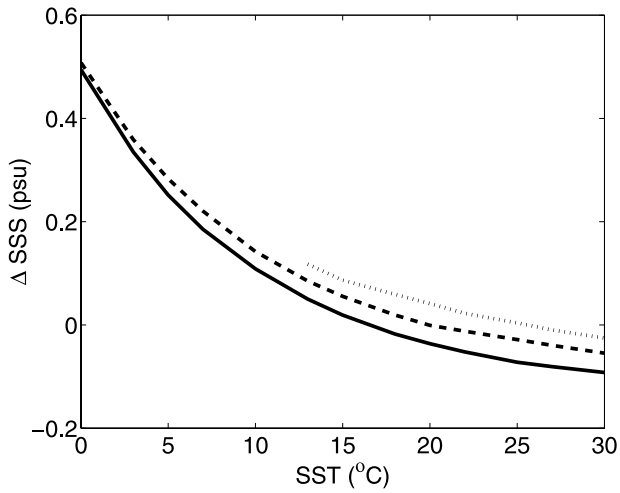

Figure 7. Δ*SSS*, error on sea surface salinity due to decoupling ϵ and wind effects, versus sea surface temperature and for various salinities: 31 (solid line), 35 (dashed line), and 38 psu (dashed-dotted line). Wind speed at 10 m is 10 m s^{-1}, and incidence angle is 0°.

reasonable precision. SSS influence on wind-induced T_b is always negligible.

3.3. Choice of a Two-Scale Cutoff Wavelength

[27] The choice of λ_d is rather arbitrary, and the influence of λ_d on simulated T_b has already been studied at higher frequencies than at L band [*Yueh*, 1997; *Trokhimovski*, 2000]. In this section we determine to what extent the choice of λ_d could be an issue for the retrieval of SSS at L band.

[28] *Irisov* [1997] showed that emission calculation with SPM is identical to emission calculation with the small slope approximation (SSA) proposed by *Voronovich* [1994]. Therefore in the case of the ocean where the slopes are always small (even in the range of long gravity waves), λ_d might be extended to infinity. Hence, whereas the small-scale wave effect is still computed with SPM/SSA, the emission from the large-scale waves might be computed with SPM/SSA instead of GO. SPM/SSA has a resonance behavior at some wavelengths in the sea wave spectrum; those resonant wavelengths get further and further away from λ_0 as incidence angles increases [*Johnson and Zhang*, 1999]. For instance, at $\theta = 50°$, there are resonant long waves up to about $10\lambda_0$. As the resonance behavior can not be reproduced with GO, it is obvious that part of the large-scale wave contribution estimated with two-scale model or with SPM/SSA model will differ. Two-scale model and SPM/SSA are not similar as long as λ_d is inside the resonance behavior range. Moreover, there are two other distinctions between second-order SPM/SSA and the two-scale model. The shadowing of the steepest waves, which is noticeable at very large incidence angles, and the hydrodynamic modulation (HM), which induces upwind/downwind asymmetry, are taken into account in two-scale model only. HM would require an expansion of the SPM/SSA higher than second order.

[29] In order to evaluate the influence of λ_d and the discrepancies between the two-scale model (SPM + GO) and the SSA, we compare T_b obtained for λ_d varying from $3\lambda_0$ to ∞ (in practice $\lambda_d = 600\lambda_0$).

[30] Figure 8 reports the difference between T_b computed in vertical polarization (T_v) with a given λ_d and T_b computed with an infinite λ_d, at $\theta = 30°$ and 40°, for a wind speed of 10 m s^{-1}. Below $\theta = 30°$, the influence of λ_d is weak, with a variation of T_b less than 0.1 K. For θ greater than 30°, variations of T_b with λ_d become noticeable. When λ_d varies from $3\lambda_0$ to $10\lambda_0$, T_b varies by up to 0.35 K in vertical polarization at 40°. In horizontal polarization (not shown), the T_b variation at 40° is almost half this value and is still less than 0.1 K for θ lower than 30°.

[31] Figure 9 shows $T_{b\ wind}$ versus wind speed, computed at $\theta = 40°$ for both polarizations with $\lambda_d = 3\lambda_0$ and $600\lambda_0$. For winds above 3 m s^{-1}, $\partial T_{b\ wind}/\partial U$ is weakly sensitive to λ_d, even at large incidence angles. In other words, the shift on $T_{b\ wind}$ between various λ_d is almost constant with U and could be removed by a correction independent of the wind speed.

[32] Because the SMOS incidence angles are mostly between 0–40°, simulations of $T_{b\ wind}$ should suffer from

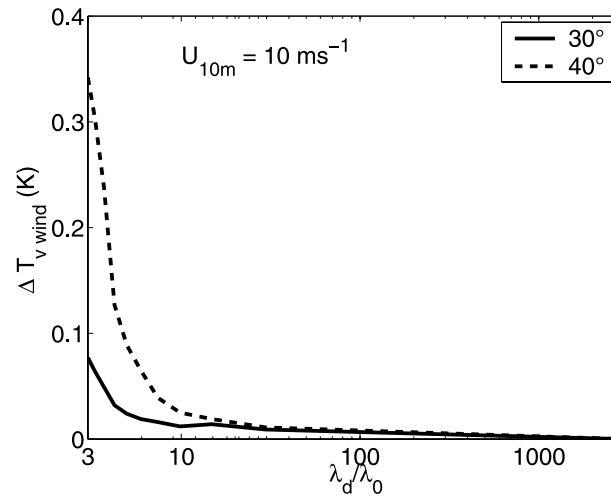

Figure 8. Influence of λ_d on T_b in vertical polarization at 30° and 40° incidence angles. Wind speed at 10 m is 10 m s^{-1}, sea surface temperature is 15°C, and sea surface salinity is 35 psu. The sea wave spectrum is DV2 (see text).

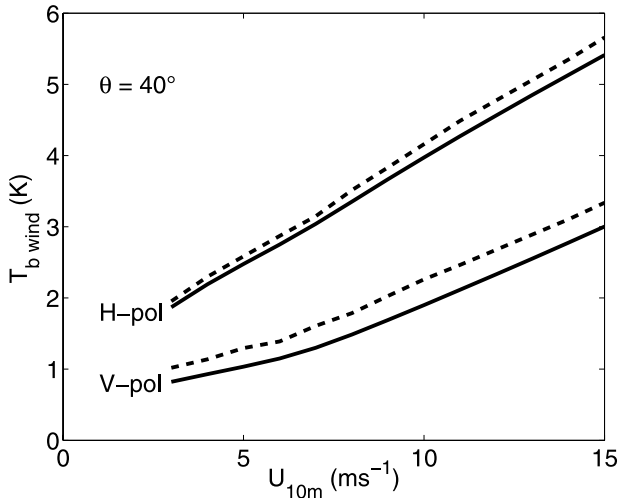

Figure 9. T_b in vertical (V-pol) and horizontal (H-pol) polarizations at 40° incidence angle versus the wind speed at 10 m for $\lambda_d = 3\,\lambda_0$ (solid line) and $\lambda_d = 600\lambda_0$ (dashed line). Sea surface temperature is 15°C, sea surface salinity is 35 psu, and the sea wave spectrum is DV2 (see text).

weak errors due to the choice of λ_d. We use $\lambda_d = 4\lambda_0$ in the following.

3.4. Influence of Sea Wave Spectrum Model in Omnidirectional Emissivity

[33] We assess to what extent various parameterizations for the sea wave spectrum affect omnidirectional $T_{b\ wind}$ (i.e., $T_{b\ wind}$ averaged over all azimuthal directions). $T_{b\ wind}$ is estimated by integrating the sea wave curvature spectrum multiplied by a weighting function which is maximum around λ_0 [*Johnson and Zhang*, 1999]. Therefore $T_{b\ wind}$ is mostly dependent on the amplitude of the sea wave spectrum around λ_0. We use the sea wave spectra introduced in section 3 to estimate T_b for various wind speeds (between 3 and 15 m s^{-1}) at various incidence angles.

[34] The largest discrepancies between the models occur for the horizontal polarization of T_b (referred as T_h) and at large incidence angles. When computed with DV or DV2 spectra, T_b varies almost linearly with the wind speed. With the Elfo spectrum, T_b exhibits a plateau between 3 and 7 m s^{-1}. Indeed, when wind speed increases from 3 to 7 m s^{-1}, the amplitude of the Elfo spectrum around $\lambda_0 = 21$ cm decreases.

[35] At nadir and moderate wind speeds (not shown), the mean sensitivity of T_b to U is 0.12, 0.17 and 0.25 $Km^{-1}s$ for the DV, Elfo and DV2 spectra respectively. Therefore, for U = 10 ms^{-1}, T_b computed with the DV2 spectrum is 1.25 K larger than the one computed with the DV spectrum. In the worst cases (i.e., for cold waters) the corresponding difference in estimated SSS is about 5 psu. When the incidence angle increases up to 40° (Figure 10), T_b sensitivity to the wind speed increases in horizontal polarization (up to 0.3 $Km^{-1}s$ with DV2 spectrum) and decreases in vertical polarization (down to 0.2 $Km^{-1}s$). The discrepancy on T_b from one spectrum model to the other may be as large as 2 K in horizontal polarization at U = 10 m s^{-1}.

[36] These results indicate that uncertainties on sea surface modeling constitute a major issue when using emissivity models in the frame of SSS retrieval. Accurate in situ measurements of the sea wave spectrum at wavelengths relevant to L band radiometry (i.e., near $\lambda = 21$ cm) would be needed to improve the accuracy of the estimate of SSS from L band radiometry.

3.5. Swell Influence on T_b

[37] The sea state is often described by the wind sea spectrum without taking into account the presence of swell. Since L band involves wavelengths larger than the ones usually used in microwave radiometry (in order to retrieve the wind speed for instance), and since *Durden and Vesecky* [1985] showed that swell could have a significant effect in L band scatterometry, we study its expected effect in L band radiometry. For this purpose,

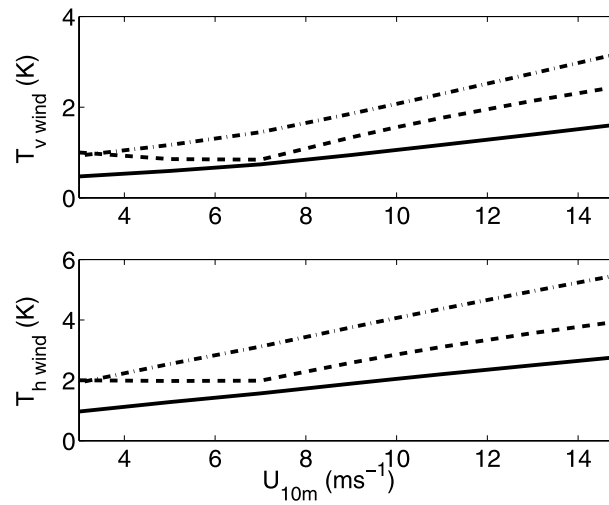

Figure 10. T_b, in (top) vertical and (bottom) horizontal polarizations, as a function of wind speed at 10 m. T_b is computed with *Durden and Vesecky* [1985] (solid line), *Elfouhaily et al.* [1997] (dashed line), and Durden and Vesecky × 2 (dashed-dotted line) spectra. Sea surface temperature is 15°C, sea surface salinity is 35 psu, and incidence angle is 40°.

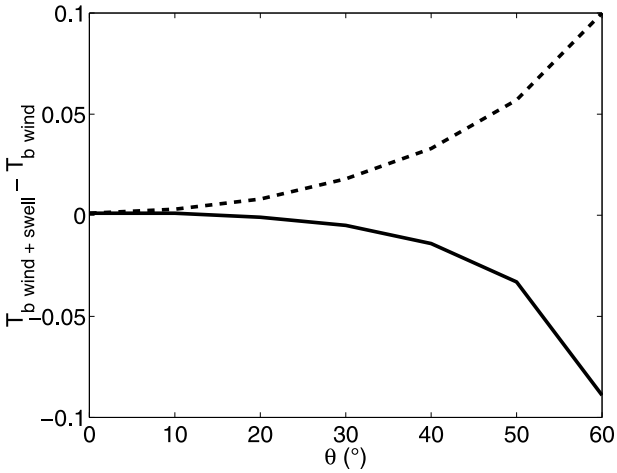

Figure 11. Influence of swell on T_b, in vertical (solid line) and horizontal(dashed line) polarizations, as a function of incidence angle. Wind speed at 10 m is 10 m s^{-1}.

we simulate a swell component by superimposing a gaussian shaped swell spectrum on the wind sea spectrum, assuming no interaction between these 2 components. The swell spectrum as a function of wave number k is

$$S(k) = \frac{h_s^2}{2\pi\sigma} \exp\left(-0.5\left(\frac{k-k_p}{\sigma}\right)^2\right) \qquad (4)$$

where h_s is the RMS height of the swell chosen equal to 1 m, k_p is the wave number of the peak of the spectrum and $\sigma = 0.0025$ m^{-1}. Figure 11 reports the difference of T_b computed with or without swell. The maximum influence is less than 0.1 K and occurs at $\theta = 60°$, which is a very large incidence angle in the SMOS context. Moreover, the azimuthal variation of T_b (not shown) is less than 0.015 K. This suggests that swell should not be noticeable on radiometric data at L band at low to moderate incidence angle (i.e., less than 40°). This however does not rule out the possibility of an indirect effect of swell, by interacting with the wind sea, and/or modifying the wave breaking and foam production. Such effects are out of the scope of this paper.

4. Discussion and Conclusion

[38] Using a two-scale sea surface emissivity model to simulate T_b at L band we explore the influence on retrieved SSS of the seawater permittivity parameterization, of the sea surface spectrum, of the choice of the two-scale cutoff wavelength and of adding swell to the wind sea.

[39] Given the requirements on retrieved SSS for oceanic studies (0.1 psu) and given the SMOS incidence angles, we find that two-scale or SPM/SSA emissivity models give similar results. Swell and the choice of cutoff wavelength are not critical issues. On another hand, the uncertainties on ϵ parameterization appear to be too large to meet the required accuracy and cannot be resolved by a constant T_b correction; new measurements of seawater permittivity are necessary especially at low temperatures. Large uncertainties also remain on the modeling of the sea wave spectrum around 21 cm, the use of various sea wave spectra leading to differences in T_b of several Kelvin for usual wind speeds. Moreover, when dealing with global ocean measurements, wind effect can not be decoupled from SST. Neglecting this coupling would induce, according to our model, significant regional biases.

[40] Another issue which has not been considered in this paper is the foam effect at L band. Nevertheless, considering the work from *Reul and Chapron* [2002; N. Reul and B. Chapron, A model of sea-foam thickness distribution for passive microwave remote sensing applications, submitted to *Journal of Geophysical Research*, 2002] and the relative large wavelength at L band with respect to the foam depth [*Droppleman*, 1970], we expect the foam influence on T_b at L band to be small especially for wind speed less than 10 m s^{-1}.

[41] **Acknowledgments.** This work was supported by CNRS (Centre National de la Recherche Scientifique), CNES (Centre National d'Etudes Spatiales) and ESA (European Space Agency). We are grateful to Alexander Voronovich and Joel Johnson for fruitful discussion about comparison between SSA and two-scale model and to Alain Weill for helpful suggestions about atmospheric boundary layer. We also thank Philippe Waldteufel and Nicolas Martin for the simulation of the SMOS field of view.

References

Antonov, J., S. Levitus, T. P. Boyer, M. Conkright, T. O' Brien, and C. Stephens, *World Ocean Atlas 1998*, vol. 1, *Temperature of the Atlantic Ocean, NOAA Atlas NESDIS 27*, 166 pp., U.S. Gov. Print. Off., Washington, D. C., 1998a.

Antonov, J., S. Levitus, T. P. Boyer, M. Conkright, T. O' Brien and C. Stephens, *World Ocean Atlas 1998*, vol. 2, *Temperature of the Pacific Ocean, NOAA Atlas NESDIS 28*, 166 pp., U.S. Gov. Print. Off., Washington, D. C., 1998b.

Antonov, J., S. Levitus, T. P. Boyer, M. Conkright, T. O' Brien, C. Stephens, and B. Trotsenko, *World Ocean Atlas 1998*, vol. 3, *Temperature of the Indian Ocean, NOAA Atlas NESDIS 29*, U.S. Gov. Print. Off., 166 pp., Washington, D.C., 1998c.

Blume, H.-J. C., A. W. Love, M. J. V. Melle, and W. W. Ho, Radiometric observations of sea temperature at 2.65 GHz over Cheasapeake Bay, *IEEE Trans. Antennas Propag.*, *25*, 121–128, 1977.

Boutin, J., E. Obligis, and E. Dinnat, WP1120, Influence of surface roughness on Tb simulated in L-band by Yueh-LODYC emissivity model and by UCL model—Analysis of the differences, *Tech. Rep. 14273/00/NL/DC*, Eur. Space Agency, Paris, 2002.

Boyer, T. P., S. Levitus, J. Antonov, M. Conkright, T. O'Brien, and C. Stephens, *World Ocean Atlas 1998*, vol. 4, *Salinity of the Atlantic Ocean, NOAA Atlas NESDIS 30*, 166 pp., U.S. Gov. Print. Off., Washington, D. C., 1998a.

Boyer, T. P., S. Levitus, J. Antonov, M. Conkright, T. O'Brien, and C. Stephens, *World Ocean Atlas 1998*, vol. 5, *Salinity of the Pacific Ocean, NOAA Atlas NESDIS 31*, 166 pp., U.S. Gov. Print. Off., Washington, D. C., 1998b.

Boyer, T. P., S. Levitus, J. Antonov, M. Conkright, T. O' Brien, C. Stephens, and B. Trotsenko, *World Ocean Atlas 1998*, vol. 6, *Salinity of the Indian Ocean, NOAA Atlas NESDIS 32*, 166 pp., U.S. Gov. Print. Off., Washington, D. C., 1998c.

Debye, P., *Polar Molecules*, Chem. Catalog Co., New York, 1929.

Dinnat, E. P., J. Boutin, G. Caudal, J. Etcheto, and P. Waldteufel, Influence of sea surface emissivity model parameters at L-band for the estimation of salinity, *Int. J. Remote Sens.*, *23*(23), 5117–5122, 2002.

Droppleman, J. D., Apparent microwave emissivity of sea foam, *J. Geophys. Res.*, *75*, 696–697, 1970.

Durden, S. L., and J. F. Vesecky, A physical radar cross-section model for a wind-driven sea with swell, *IEEE J. Oceanic Eng.*, *OE-10*, 445–451, 1985.

Elfouhaily, T., B. Chapron, K. Katsaros, and D. Vandemark, A unified directional spectrum for long and short wind-driven waves, *J. Geophys. Res.*, *102*, 15,781–15,796, 1997.

Ellison, W. J., A. Balana, G. Delbos, K. Lamkaouchi, L. Eymard, C. Guillou, and C. Prigent, Study and measurement of the dielectric properties of sea water, *Tech. Rep. 11197/94/NL/CN*, Eur. Space Agency, Paris, 1996.

Ho, W. W., and W. F. Hall, Measurements of the dielectric properties of seawater and NaCl solutions at 2.65 GHz, *J. Geophys. Res.*, *78*, 6301–6315, 1973.

Ho, W. W., A. W. Love, and M. J. V. Melle, Measurements of the dielectric properties of sea water at 1.43 GHz, *Tech. Rep. CR-2458*, NASA, Washington, D. C., 1974.

Hollinger, J. P., Passive microwave measurements of sea surface roughness, *IEEE Trans. Geosci. Electronics*, *9*, 165–169, 1971.

Irisov, V. G., Small-slope expansion for thermal and reflected radiation from a rough surface, *Waves Random Media*, *7*, 1–10, 1997.

Johanessen, J., et al., Scientific requirements and impact of space observation of ocean salinity for modeling and climate studies, *Tech. Rep. 14273/00/NL/DC*, Eur. Space Agency, Paris, 2002.

Johnson, J. T., and M. Zhang, Theoretical study of the small slope approximation for ocean polarimetric thermal emission, *IEEE Trans. Geosci. Remote Sens.*, *37*, 2305–2316, 1999.

Kerr, Y. H., et al., SMOS-MIRAS on RAMSES: Radiometry applied to soil moisture and salinity measurements, full proposal, A.O. Earth Explorer Opportunity Missions, Eur. Space Agency, Paris, 1998.

Klein, L. A., and C. T. Swift, An improved model for the dielectric constant of sea water at microwave frequencies, *IEEE Trans. Antennas Propag.*, *25*, 104–111, 1977.

Le Vine, D. M., M. Kao, R. W. Garvine, and T. Sanders, Remote sensing of ocean salinity: Results from the Delaware coastal current experiment, *J. Atmos. Oceanic Technol.*, *15*, 1478–1484, 1998.

Miller, J. L., M. A. Goodberlet, and J. B. Zaitzeff, Airborne salinity mapper makes debut in coastal zone, *Eos Trans. AGU*, *79*, 173–177, 1998.

Reul, N., and B. Chapron, WP1300, Foam emissivity modeling, *Tech. Rep. 14273/00/NL/DC*, Eur. Space Agency, Paris, 2002.

Sasaki, Y., I. Asanuma, K. Muneyama, G. Naito, and T. Suzuki, The dependence of sea-surface microwave emission on wind speed, frequency, incidence angle, and polarization over the frequency range from 1 to 40 GHz, *IEEE Trans. Geosci. Remote Sens.*, *25*, 138–146, 1987.

Stogryn, A., Equations for calculating the dielectric constant of saline water, *IEEE Trans. Microwave Theory Techniques*, *19*, 733–736, 1971.

Stogryn, A., Equations for the permittivity of sea water, technical report, GenCorp Aerojet, Sacramento, Calif., 1997.

Stogryn, A. P., H. T. Bull, K. Rubayi, and S. Iravanchy, The microwave dielectric properties of sea and fresh water, technical report, GenCorp Aerojet, Sacramento, Calif., 1995.

Swift, C. T., Microwave radiometer measurements of the Cape Cod Canal, *Radio Sci.*, *9*, 641–653, 1974.

Trokhimovski, Y. G., Gravity-capillarity wave curvature spectrum and mean-square slope retrieved from microwave radiometric measurements (Coastal Ocean Probing Experiment), *J. Atmos. Oceanic Technol.*, *17*, 1259–1270, 2000.

Voronovich, A. G., *Wave Scattering From Rough Surfaces, Wave Phenomena Ser.*, vol. 17, 2nd ed., Springer-Verlag, New York, 1994.

Waldteufel, P., and G. Caudal, Off-axis radiometric measurements; application to interferometric antenna designs, *IEEE Trans. Geosci. Remote Sens.*, *40*(6), 1435–1439, 2002.

Waldteufel, P., J. Boutin, and Y. Kerr, Selecting an optimal configuration for the Soil Moisture and Ocean Salinity mission, *Radio Sci.*, *38*(3), 8051, doi:10.1029/2002RS002744, 2003.

Webster, W. J. Jr., and T. T. Wilheit, Spectral characteristics of the microwave emission from a wind-driven foam-covered sea, *J. Geophys. Res.*, *81*, 3095–3099, 1976.

Wilson, W. J., S. H. Yueh, S. J. Dinardo, S. L. Chazanoff, A. Kitiyakara, F. K. Li, and Y. Rahmat-Samii, Passive active

L- and S-band (PALS) microwave sensor for ocean salinity and soil moisture measurements, *IEEE Trans. Geosci. Remote Sens.*, *39*, 1039–1048, 2001.

Yueh, S. H., Modeling of wind direction signals in polarimetric sea surface brightness temperatures, *IEEE Trans. Geosci. Remote Sens.*, *35*, 1400–1418, 1997.

Yueh, S. H., R. West, W. J. Wilson, F. K. Li, E. G. Njoku, and Y. Rahmat-Samii, Error sources and feasibility for microwave remote sensing of ocean surface salinity, *IEEE Trans. Geosci. Remote Sens.*, *39*, 1049–1060, 2001.

Zhang, M., and J. T. Johnson, Comparison of modeled and measured second azimuthal harmonics of ocean surface brightness temperatures, *IEEE Trans. Geosci. Remote Sens.*, *39*, 448–452, 2001.

J. Boutin, E. P. Dinnat, and J. Etcheto, Laboratoire d'Océanographie Dynamique et de Climatologie, Tour 14-15 2ème étage, boîte 100, Université Pierre et Marie Curie, 4 place Jussieu, 75252 Paris, France. (jb@lodyc.jussieu.fr; dinnat@lodyc.jussieu.fr; je@lodyc.jussieu.fr)

G. Caudal, Centre d'étude des Environnements Terrestres et Planétaires, I.U.T. de Vélizy 10-12 avenue de l'Europe, 78140 Vélizy, France. (gca@cetp.ipsl.fr)

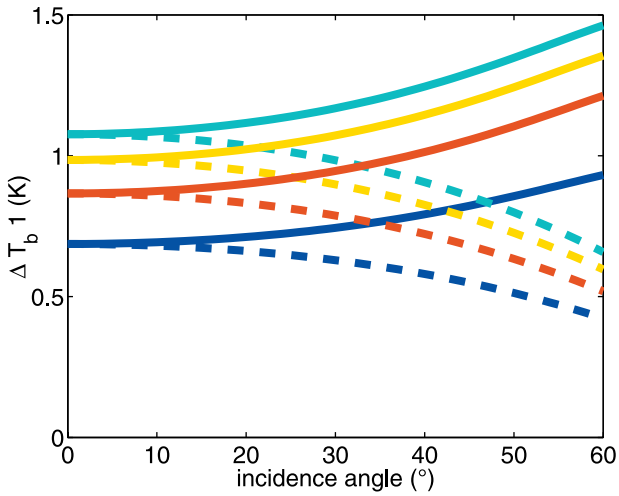

Figure 3. Differences of $T_{b\ flat}$ estimated with EL and KS models (EL-KS) versus the incidence angle, in vertical polarization (solid line) and horizontal polarization (dashed line). Sea surface temperature is 0°C (dark blue), 10°C (light blue), 20°C (yellow) and 30°C (red).

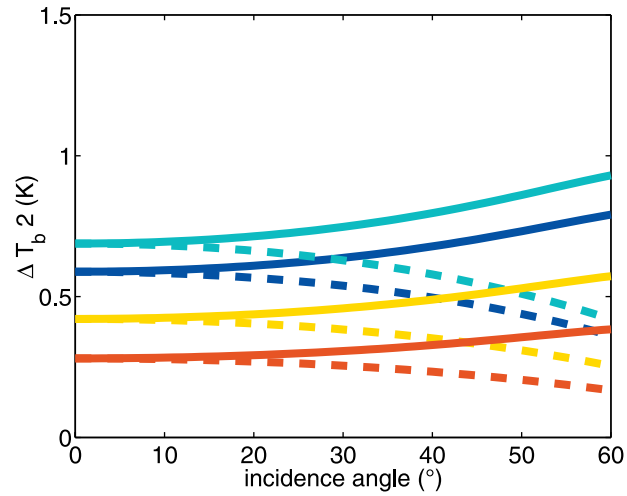

Figure 4. Differences of $T_{b\ flat}$ estimated with S95 and KS models (S95-KS) versus the incidence angle, in vertical polarization (solid line) and horizontal polarization (dashed line). Sea surface temperature is 0°C (dark blue), 10°C (light blue), 20°C (yellow), and 30°C (red).